ACCEPTED FOR THE PUBLICATION IN THE *Astrophysical Journal Letters*
Preprint typeset using LaTeX style emulateapj v. 25/04/01

0103−72.6: A NEW OXYGEN-RICH SUPERNOVA REMNANT IN THE SMALL MAGELLANIC CLOUD

SANGWOOK PARK[1], JOHN P. HUGHES[2], DAVID N. BURROWS[1], PATRICK O. SLANE[3], JOHN A. NOUSEK[1], AND GORDON P. GARMIRE[1]

Accepted for the publication in the Astrophysical Journal Letters

ABSTRACT

0103−72.6, the second brightest X-ray supernova remnant (SNR) in the Small Magellanic Cloud (SMC), has been observed with the *Chandra X-Ray Observatory*. Our *Chandra* observation unambiguously resolves the X-ray emission into a nearly complete, remarkably circular shell surrounding bright clumpy emission in the center of the remnant. The observed X-ray spectrum for the central region is evidently dominated by emission from reverse shock-heated metal-rich ejecta. Elemental abundances in this ejecta material are particularly enhanced in oxygen and neon, while less prominent in the heavier elements Si, S, and Fe. We thus propose that 0103−72.6 is a new "oxygen-rich" SNR, making it only the second member of the class in the SMC. The outer shell is the limb-brightened, soft X-ray emission from the swept-up SMC interstellar medium. The presence of O-rich ejecta and the SNR's location within an HII region attest to a massive star core-collapse origin for 0103−72.6. The elemental abundance ratios derived from the ejecta suggest an $\sim$18 $M_\odot$ progenitor star.

Subject headings: ISM: individual (0103−72.6) — supernova remnants — X-rays: ISM

1. INTRODUCTION

Identifying the explosion type of a supernova remnant (SNR), largely between the thermonuclear (Type Ia) and the core-collapse (Type II or Ib/Ic) explosions, is difficult, yet important for understanding how heavy elements are synthesized and distributed into interstellar space. A small number of SNRs are known to exhibit emission from SN ejecta material which is enhanced in O, Ne, and Mg. Based on the nucleosynthesis products of such explosions, these "oxygen-rich" SNRs result from the core-collapse of massive progenitor stars. The O-rich SNRs thus provide a useful test-ground for the studies of SN nucleosynthesis. The number of known O-rich SNRs is small, however: there are three in the Galaxy (Cassiopeia A, Puppis A, and G292.0+1.8), two (N132D and 0540−69.3) in the Large Magellanic Cloud (LMC), and merely one (0102.2−7219) in the Small Magellanic Cloud (SMC). Although these SNRs are all classified as O-rich SNRs by virtue of the presence of ejecta material enriched in O, the nature of the individual objects varies significantly from one to another. The detection of more such SNRs is thus required for unbiased, systematic investigations of this interesting class of SNRs.

0103−72.6 is the second brightest X-ray SNR in the SMC (Seward & Michell 1981; Haberl et al. 2000). The X-ray images taken with the *ROSAT*/HRI showed a centrally-peaked morphology and a faint outer shell with an $\sim 3'$ diameter (Yokogawa et al. 2002). The radio data indicated only a faint shell-like feature roughly along the X-ray shell (Mills et al. 1982; Yokogawa et al. 2002). In the optical band, 0103−72.6 is very faint, probably elliptical, and ring-like with nearly the same angular size as the X-ray and the radio remnant (Mathewson et al. 1983). Although the large angular size was suggestive of a relatively old age ($\sim 10^4$ yr), the *ASCA* data suggested elevated metal abundances (Yokogawa et al. 2002). The chemical compositions of the overabundant material were consistent with a core-collapse Type II SN nucleosynthesis model. This result was also supported by the SNR's location within an HII region (DEM S125) (e.g., Filipović et al. 1998 and references therein), which is consistent with a massive progenitor.

We report here on the results from our observation of 0103−72.6 with the *Chandra X-Ray Observatory*. The high resolution *Chandra* data unambiguously resolve the SNR into a limb-brightened circular shell surrounding bright, clumpy central emission. The central regions are enriched in O and Ne whereas the outer shell is dominated by emission from the swept-up SMC ISM with low elemental abundances. Based on these results, we propose that 0103−72.6 is a new O-rich SNR in the SMC.

2. OBSERVATION & DATA REDUCTION

We observed SNR 0103−72.6 with the Advanced CCD Imaging Spectrometer (ACIS) on board the *Chandra X-Ray Observatory* on 2002 August 27 as part of the Guaranteed Time Observation program. The ACIS-S3 chip, with very faint (VFAINT) mode, was chosen. We screened the raw data in order to utilize the VFAINT mode and then filtered by the flight timeline filter. We corrected the charge transfer inefficiency (CTI; Townsley et al. 2000) with the methods developed by Townsley et al. (2002a). The data were then screened by the standard filtering with status and grade. We inspected the overall lightcurve for any background flares. We found no significant variations of the lightcurve for the $\sim 3'$ diameter source region. After this data reduction, the effective exposure was $\sim$49 ks with $\sim$45000 photons in the 0.3−3 keV band. The overall spectrum of 0103−72.6 is very soft and *all* source photons are detected at $E < 3$ keV.

3. X-RAY IMAGES

Figure 1 is a "true-color" image of SNR 0103−72.6. The high resolution ACIS images clearly resolve the bright central emission and the limb-brightened outer shell. The outer shell is remarkably circular and dominated by soft X-ray emission, indicated in red. The morphological and spectral features of the circumferential shell are typical of X-ray emission from ISM

[1] Department of Astronomy and Astrophysics, Pennsylvania State University, 525 Davey Laboratory, University Park, PA. 16802; park@astro.psu.edu
[2] Department of Physics and Astronomy, Rutgers University, 136 Frelinghuysen Road, Piscataway, NJ. 08854-8019
[3] Harvard-Smithsonian Center for Astrophysics, 60 Garden Street, Cambridge, MA. 02138

swept-up by the blast wave shock front. In contrast, the central regions are bright in all colors and show a complex mixture of X-ray emitting knots. These features are qualitatively consistent with a Sedov picture.

We explored the angular distributions of the X-ray line emission by constructing *equivalent width* (EW) images for the detected elemental species, following the method of Park et al. (2002). We generated EW images for O and Ne by selecting photons around the broad line features. We present the O EW image in Figure 2. The O EW image clearly reveals enhancements in O line emission in the central regions of 0103−72.6. In contrast, the circumferential shell is fairly featureless in the O EW image. These overall features are also consistent in the Ne EW image. These EW features support our conjecture regarding the overall characteristics of the SNR based on the color images: i.e., the central regions are emission from metal-rich ejecta heated by the reverse shock, and the outer shell is the emission from the forward shock sweeping through the ambient ISM.

4. X-RAY SPECTRA

The high resolution ACIS images allow us to perform a spatially-resolved spectral analysis of 0103−72.6. For the spectral analysis, we use detector response matrices, as generated by Townsley et al. (2002b), appropriate for our CTI-corrected data. The low energy ($E \lesssim 1$ keV) quantum efficiency (QE) of the ACIS has degraded because of molecular contamination on the optical blocking filter. We corrected this time-dependent QE degradation by modifying the ancillary response function for each extracted spectrum, utilizing the IDL ACISABS software[4].

The presence of the limb-brightened shell, which is remarkably circular around the centrally-bright emission, indicates a significant contribution from the foreground/background swept-up ISM to the central excess emission. In order to characterize this projected emission from the heated ISM, we first extracted spectra from the bright parts of the limb-brightened circumferential shell ("SW shell" and "SE shell" regions in Figure 3). This outer shell is most likely dominated by emission from the blast wave shock front. We thus fitted these spectra simultaneously with a nonequilibrium ionization (NEI) plane-parallel shock model (Borkowski et al. 2001) (Figure 4). Only the normalization was varied freely for each individual regional spectrum. These outer shell spectra can be best-fitted with $kT \sim 0.25-0.30$ keV, depending on the implied foreground column, which is poorly constrained ($N_H < 1.2 \times 10^{21}$ cm^{-2}). The fitted metal abundances are low ($\sim$0.1 solar), which is in agreement with typical SMC ISM (Russell & Dopita 1992).

We then extracted spectra from the east and the west side of the central excess emission, *interior* to the outer shell (i.e., "east" and "west" regions in Figure 3). We simultaneously fitted these spectra with an NEI Sedov model assuming that the electron temperature immediately behind the shock is $kT \sim 0.25-0.3$ keV as obtained from the outer shell spectrum. Only the normalizations were allowed to vary independently. While the Sedov model corresponds to the full temperature and density distribution of the swept-up component of an entire SNR, we use this model as a first-order approximation to account for the expected temperature distribution for the plasma in the SNR's interior. The goal of these fits is to describe the projected blast wave emission seen in the central region in combination with the ejecta component. These spectra can be described by $kT \sim 0.26$ keV and low SMC-like abundances of $0.12^{+0.08}_{-0.04}$ solar (Figure 4; Table 1).

The central region spectrum has been extracted from the "center" region (Figure 3). We fitted this spectrum with a two-component model: i.e., a Sedov component for the projected emission from the swept-up ISM, and a plane-shock model for the central ejecta component (Figure 5). We fixed the Sedov component parameters at the best-fit values obtained above. This Sedov component for the projected emission from the swept-up ISM comprises $\sim$15% of the observed flux for the "center" region. The best-fit ejecta electron temperature ($kT \sim 0.53$ keV) is higher than that of the blast wave shock front as measured from the outer shell (Table 1). The elemental abundances for the ejecta component were varied freely for O, Ne, Mg, Si and Fe while others are fixed at the SMC values (Russell & Dopita 1992). The fitted abundances are also higher than those of the SMC: particularly, O and Ne abundances are 4−6 times higher than typical SMC abundances. Mg and Si are moderately elevated ($\sim$1.5 times the SMC), and Fe abundance ($\sim$0.3 times the SMC) is very low. The S abundance is unconstrained with the current data and thus fixed at the SMC abundance. The improvement made by fitting the S abundance is statistically negligible.

5. DISCUSSION

The X-ray spectrum from the bright central region of 0103−72.6 indicates the presence of ejecta material which is particularly enriched in O and Ne. We thus propose that 0103−72.6 is a new O-rich SNR, based on the results of our X-ray spectral analysis. 0103−72.6 is then the second member of this class in the SMC in addition to SNR 0102.2−7219 (Dopita & Tuohy 1984). The O- and Ne-dominated nature of the ejecta of 0103−72.6, with the relative absence of high-Z species, particularly Fe, is similar to that of 0102.2−7219 (Blair et al. 2000; Sasaki et al. 2001) and the Galactic O-rich SNR G292.0+1.8 (Park et al. 2003a). This abundance distribution however differs from that of Cas A, which shows significant Si-, S-, and Fe-rich ejecta (Hughes et al. 2000a). The physical location within an HII region and the detected O-rich nature are typical signatures of a core-collapse origin for 0103−72.6. We thus compare the measured elemental abundances of 0103−72.6 with a Type II SN nucleosynthesis model (Table 2). Although the measured elemental abundances have systematic uncertainties depending on the embedded contribution from the background swept-up ISM component, the quoted abundance ratios are nearly independent of these uncertainties. The measured abundance ratios are in plausible agreement with a Type II nucleosynthesis model for an 18 $M_\odot$ progenitor star.

Assuming that 0103−72.6 is in the Sedov phase, we may derive the SNR parameters by taking advantage of the spatial information obtained by the high-resolution ACIS images. Based on the best-fit volume emission measure ($EM = 5.4 \times 10^{58}$ cm^{-3} by combining four fitted shell regions; Table 1), we derive the postshock electron density, $n_e = 0.79$ cm^{-3} for the blast wave shock front. In this estimation, we have assumed that the average outer radius of the SNR is $R \sim 85''$ (corresponding to $\sim$24.7 pc at $d = 60$ kpc) and that the blast wave shell is $\sim 20''$ thick, based on the ACIS image. The

[4] For the discussion on this instrumental issue, see http://cxc.harvard.edu/cal/Acis/Cal_prods/qeDeg/index.html. The software was developed by George Chartas and is available at http://www.astro.psu.edu/users/chartas/xcontdir/xcont.html.

average depth through our shell regions is then ∼23 pc which implies a total volume for the four shell regions of $\sim 1 \times 10^{59}$ cm^3. The pre-shock hydrogen density is then $n_0 \sim 0.16$ cm^{-3} assuming a factor of 4 density compression behind shock and a mean charge state of $n_e = 1.2\, n_H$. Assuming uniform density for the ambient ISM, we estimate the mass swept-up by the blast wave to be $M_{swept} \sim 570$ M$_\odot$. The best-fit electron temperature of the shock front (kT = 0.3 keV) corresponds to a shock velocity of $v \sim 480$ km s^{-1}, under the assumption of electron-ion temperature equilibration. We then derive the SNR age of $t \sim 1.8 \times 10^4$ yr and the SN explosion energy of $E_0 \sim 1.2 \times 10^{51}$ ergs based on the Sedov solution. 0103−72.6 thus appears to be the oldest known example of an O-rich SNR. The detection of significant amounts of ejecta material in 0103−72.6 adds yet another such an example of the growing number of middle-aged SNRs with observable ejecta (e.g., Park et al. 2003b and references therein).

We make a brief morphological comparison between the two SMC O-rich SNRs, 0103−72.6 and 0102.2−7219. 0102.2−7219 is a young SNR (∼10^3 yr) with a small angular size of ∼44″ diameter, and the X-ray morphology shows a bright ring-like structure embedded in a relatively faint diffuse emission extending beyond the bright ring (Gaetz et al. 2000). This morphology was interpreted as the reverse shock front heating the central O-rich ejecta material (i.e., the sharp inner boundary of the bright ring) and the blast wave shock front propagating into the ambient ISM (i.e., the outer boundary of the faint extended diffuse emission) (Gaetz et al. 2000). In comparison, as we have just determined, 0103−72.6 has a larger angular size (190″) and is significantly older (1.8×10^4 yr). The reverse shock-heated ejecta material shows a relatively well-defined, but complex structure near the center of the SNR. The blast wave shock front is represented by the limb-brightened, soft shell-like feature surrounding the central ejecta. It appears that the reverse shock has reached the center of the SNR in 0103−72.6, while it has reached only ∼60% of the current blast wave shock radius in 0102.2−7219 (Gaetz et al. 2000). The blast wave shock front of 0103−72.6 has swept up significant amounts of ambient ISM and slowed down ($v \sim 480$ km s^{-1}) to produce a limb-brightened soft X-ray shell, whereas 0102.2−7219 shows a high velocity ($v \sim 6000$ km s^{-1}; Hughes et al. 2000b) shock front without significant limb-brigtening and presumably less swept-up ISM. Both of the SNRs have a remarkably circular outer boundary, and thus likely uniform surrounding ISM distributions. The morphological characteristics of these two SMC SNRs then appear to be primarily caused by the substantial difference in the ages (∼10^3 yr vs. ∼10^4 yr): i.e., 0103−72.6 appears to be a more evolved version of 0102.2−7219.

This work has been supported in parts by NASA contract NAS8-01128. JPH was supported by *Chandra* grants GO2-3069X and GO3-4086X. POS was supported by NASA contract NAS8-39073.

REFERENCES

Anders, E., & Grevesse, N. 1989, Geochimica et Cosmochimica Acta, 53, 197
Blair, W. P., Morse, J. A., Raymond, J. C. et al. 2000, ApJ, 537, 667
Borkowski, K. J., Lyerly, W. J., & Reynolds, S. P. 2001, ApJ, 548, 820
Dopita, M. A., & Tuohy, I. R. 1984, ApJ, 282, 135
Filipović, M. D., Pietsch, W., Haynes, R. F. et al. 1998, A&AS, 127, 119
Gaetz, T. J., Butt, Y. M., Edgar, R. et al. 2000, ApJ, 534, L47
Haberl, F., Filipović, M. D., Pietsch, W., & Kahabka, P. 2000, A&AS, 142, 41
Hughes, J. P., Rakowski, C. E., Burrows, D. N. et al. 2000a, ApJ, 528, L109
Hughes, J. P., Rakowski, C. E., & Decourchelle, A. 2000b, ApJ, 543, L61
Mathewson, D. S., Ford, V. L., Dopita, M. A. et al. 1983, ApJS, 51, 345
Mills, B. Y., Little, A. G., Durdin, J. M. et al. 1982, MNRAS, 200, 1007
Nomoto, K., Hashimoto, M., Tsujimoto, T. et al. 1997, Nucl. Phys. A, 616, 79c
Park, S., Roming, P. W. A., Hughes, J. P. et al. 2002, ApJ, 564, L39
Park, S., Hughes, J. P., Slane, P. O. et al. 2003a, ApJL, Submitted
Park, S., Hughes, J. P., Slane, P. O. et al. 2003b, ApJ, 592, L41
Russell, S. C., & Dopita, M. A., 1992, ApJ, 384, 508
Sasaki, M., Stadlbauer, F. X., Haberl, F. et al. 2001, A&A, 365, L237
Seward, F. D., & Michell, M. 1981, ApJ, 243, 736
Thielemann, F.-K, Nomoto, K., & Hashimoto, M.-A. 1996, ApJ, 460, 408
Townsley, L. K., Broos, P. S., Garmire, G. P. et al. 2000, ApJ, 534, L139
Townsley, L. K., Broos, P. S., Nousek, J. A. et al. 2002a, Nuclear Instruments & Methods in Physics Research Section A, 486, 751
Townsley, L. K., Broos, P. S., Chartas, G. et al. 2002b, Nuclear Instruments & Methods in Physics Research Section A, 486, 716
Yokogawa, J., Imanish, K., Koyama, K. et al. 2002, PASJ, 54, 53

TABLE 1
SPECTRAL PARAMETERS OF 0103−72.6.

	ISM[a]	Ejecta[b]
N_H (10^{21} cm^{-2})	< 1.2	$1.1^{+0.6}_{-0.4}$
kT (keV)	$0.30^{+0.12}_{-0.05}$	$0.53^{+0.25}_{-0.18}$
$n_e t$ (10^{11} cm^{-3} s)	$1.6^{+1.2}_{-0.7}$	$1.4^{+0.3}_{-0.3}$
EM (10^{58} cm^{-3})	$5.4^{+1.1}_{-1.1}$	$0.8^{+0.3}_{-0.3}$
χ^2/ν	169.0/137	86.7/58

[a]The best-fit plane-shock model from the combined four shell regions.

[b]The plane-shock component of the center region.

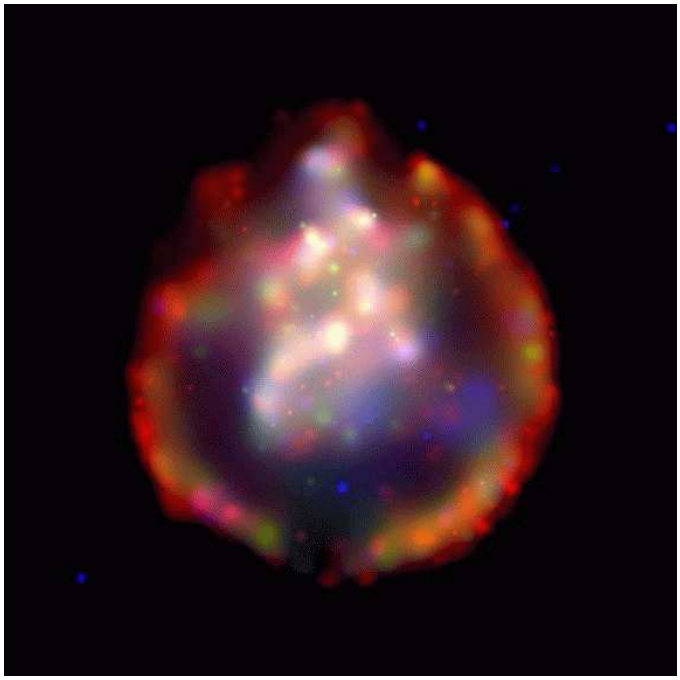

FIG. 1.— The true-color ACIS image of 0103−72.6. The red is 0.3−0.75 keV, the green is 0.75−0.99 keV, and the blue is 0.99−3.0 keV band images. Each broad-subband image has been adaptively smoothed. We note that the bright clumpy features in the central region are real structures which were resolved by the ACIS (see Figure 3). We however caution that faint, compact clumps (∼arcsec scale) along the outer shell are likely artifacts caused by the adaptive smoothing.

TABLE 2
COMPARISONS OF THE ABUNDANCE RATIOS.

Abundance Ratio	Center 0103−72.6	SMC[a]	Model[b] 15 $M_\odot$	18 $M_\odot$	20 $M_\odot$	25 $M_\odot$	40 $M_\odot$
O/Ne	$4.1^{+1.2}_{-1.1}$	5.8	13.0	5.3	7.1	5.9	16.0
O/Mg	$31.5^{+12.5}_{-14.7}$	11.2	15	24	12	19	26
O/Si	$27.1^{+12.8}_{-14.9}$	10.0	7.9	15	25	45	136

[a]Russell & Dopita (1992).

[b]Type II SN nucleosynthesis model by Nomoto et al. (1997).

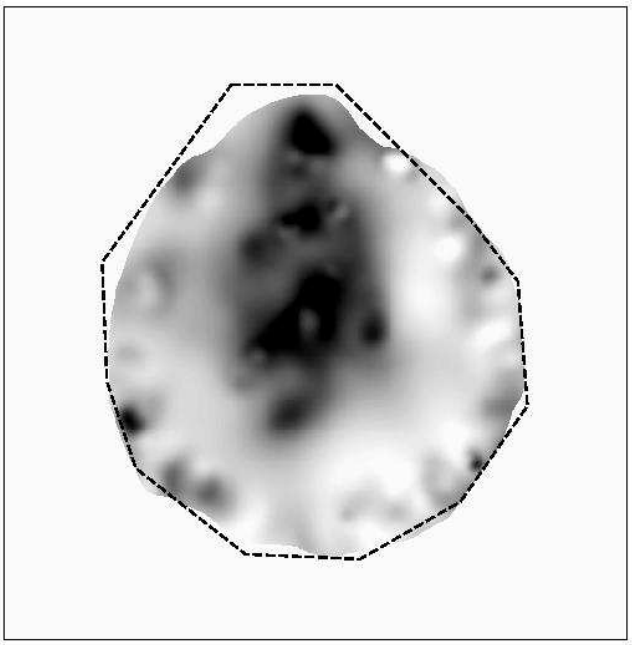

FIG. 2.— The linear gray-scale O EW image of SNR 0103−72.6, comprised of combined O Heα and O Lyα lines. The darker gray-scales indicate high EWs: i.e., ∼500−650 eV around the central regions, and ∼150−300 eV otherwise. The line emission was extracted from E = 500−720 eV. The underlying continuum was from E = 300−450 eV and E = 760−850 eV, and then logarithmically interpolated to the mean line energy of 575 eV. Both line and continuum images have been adaptively smoothed before the calculation of the EW. The EWs were set to zero near the boundary of the SNR (as marked with a dashed line) in order to avoid the noise caused by low background photon statistics.

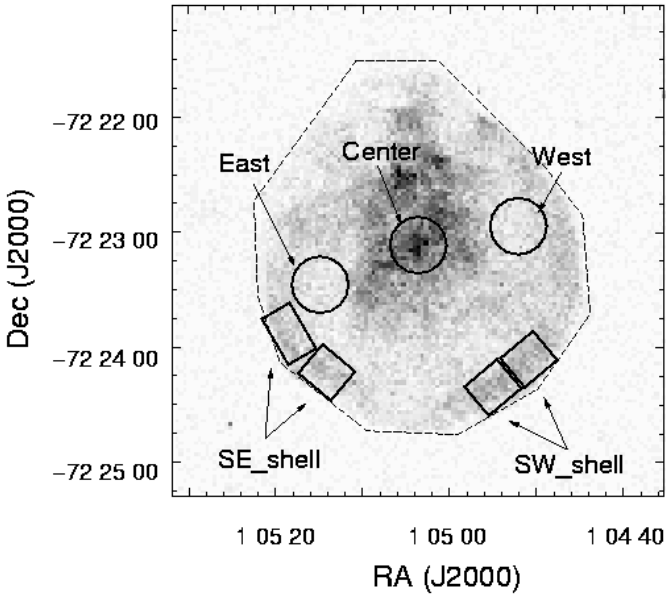

FIG. 3.— The gray-scale broadband image of SNR 0103−72.6. The image has been rebinned by 4 pixels for the purpose of display. Darker gray-scales are higher intensities. Regions used for the spectral analysis are marked.

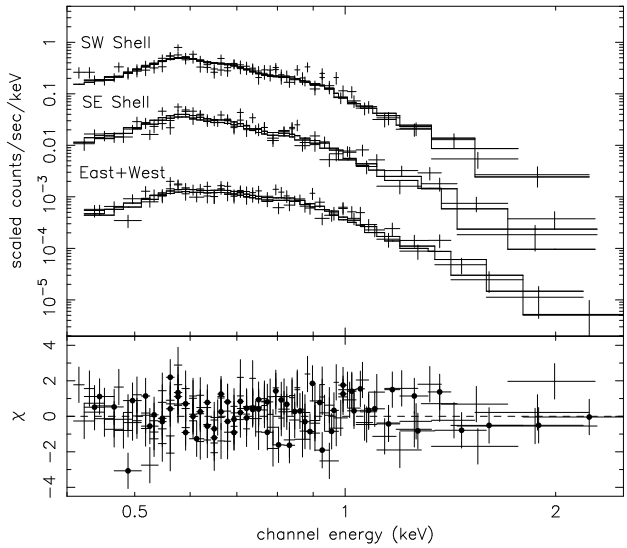

FIG. 4.— X-ray spectrum from the swept-up ISM of 0103−72.6. The individual flux levels have been arbitrarily scaled for the purpose of display. In the lower panel, residuals from the best-fit model for the east+west regions are presented with filled-circles, while those for the shell regions are presented as data points without filled-circles.

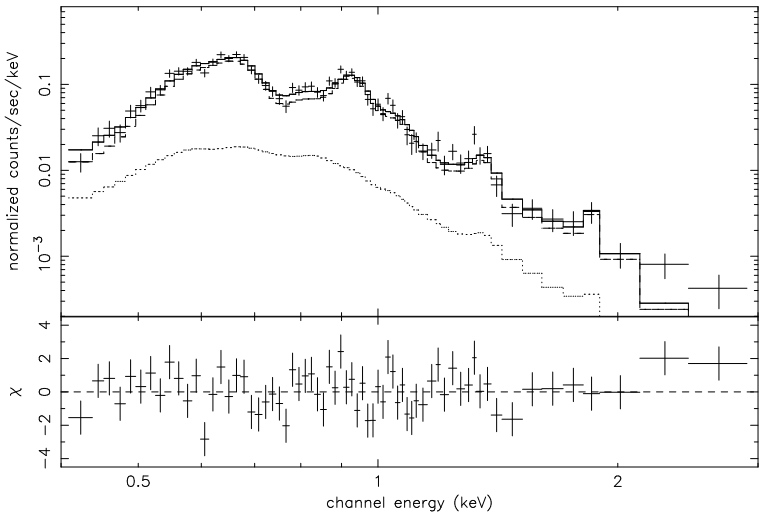

FIG. 5.— X-ray Spectrum of the O-rich ejecta as extracted from the “center” region. The projected emission from the swept-up ISM has been included with a Sedov component (the dotted line).